

# The effect of confining impermeable boundaries on gravity currents in a porous medium

MADELEINE J. GOLDING† AND HERBERT E. HUPPERT

Institute of Theoretical Geophysics, Department of Applied Mathematics and Theoretical Physics,  
University of Cambridge, Wilberforce Road, Cambridge CB3 0WA, UK

(Received 3 June 2009; revised 2 November 2009; accepted 2 November 2009)

The effect of confining boundaries on gravity currents in porous media is investigated theoretically and experimentally. Similarity solutions are derived for currents when the volume increases as  $t^\alpha$  in horizontal channels of uniform cross-section with boundary height  $b$  satisfying  $b \sim a|y/a|^n$ , where  $y$  is the cross-channel coordinate and  $a$  is a length scale of the channel width. Experiments were carried out in V-shaped and semicircular channels for the case of gravity currents with constant volume ( $\alpha = 0$ ) and constant flux ( $\alpha = 1$ ). These showed generally good agreement with the theory.

Typically, we find that the propagation of the current is well described by  $L \sim t^c$  for some scalar  $c$ . We study the dependence of  $c$  on the time exponent of the volume of fluid in the current,  $\alpha$ , and the geometry of the channel, parameterized by  $n$ . For all channel shapes, there exists a critical value of  $\alpha$ ,  $\alpha_c = 1/2$ , above which increasing  $n$  causes an increase in  $c$  and below which increasing  $n$  causes a decrease in  $c$ , where increasing  $n$  corresponds to opening up the channel boundary to the horizontal. The current height increases or decreases with respect to time depending on whether  $\alpha$  is greater or less than  $\alpha_c$ . It is this fact, along with global mass conservation, which explains why varying the channel shape  $n$  affects the propagation rate  $c$  in different ways depending on  $\alpha$ .

We also consider channels inclined at an angle  $\theta$  to the horizontal. When the slope of the channel is much greater than the slope of the free surface of the current, the component of gravity parallel to the slope dominates, causing the current to move with a constant velocity,  $V_f$  say, regardless of channel shape  $n$  and flux parameter  $\alpha$ , in agreement with results for a two-dimensional gravity current obtained by Huppert & Woods (1995) and some initially axisymmetric gravity currents presented by Vella & Huppert (2006). If the effect of the component of gravity perpendicular to the channel may not be neglected, i.e. if the slopes of the channel and free surface of the current are comparable, we find that, in a frame moving with speed  $V_f$ , the form of the governing equation for the height of a current in an equivalent horizontal channel is recovered. We calculate that the height of a constant flux gravity current down an inclined channel will tend to a fixed depth, which is determined by the channel shape,  $n$ , and the physical properties of the fluid and rock. Experimental and numerical results for inclined V-shaped channels agree very well with this theory.

---

† Email address for correspondence: mjpg88@cam.ac.uk

## 1. Introduction

Gravity currents occur when a fluid of one density intrudes into a fluid of a different density. The motion, which is predominantly horizontal, is driven by gravity acting on the different densities. An extensive amount of work has been carried out investigating the behaviour of gravity currents in different physical situations (see, e.g. Simpson 1997; Huppert 2006). Factors that affect the motion of a gravity current include the physical and chemical properties of the current and its surroundings, the volume of the current and the nature and orientation of its confining boundaries.

The behaviour of gravity currents in porous media has been studied in previous work for two-dimensional and several three-dimensional geometries and is often analysed using the condition that the volume of fluid in the current is given at any time by  $V(t) = Qt^\alpha$  for some constants  $Q > 0$  and  $\alpha \geq 0$ . A two-dimensional gravity current in a porous medium over a horizontal lower boundary propagates like  $t^{(\alpha+1)/3}$ , while down a slope that is much steeper than the slope of the current surface, it propagates linearly with time (Huppert & Woods 1995). An axisymmetric current over a horizontal boundary spreads like  $t^{(\alpha+1)/4}$  (Lyle *et al.* 2005), while the front position of an initially axisymmetric current moving over an inclined flat boundary depends on the value of  $\alpha$  (Vella & Huppert 2006). For  $\alpha < 3$ , it propagates axisymmetrically at short times, with the radius proportional to  $t^{(\alpha+1)/4}$ , and at long times the current spreads predominantly downslope, like  $t$ . This behaviour is reversed for  $\alpha > 3$ , with the current spreading predominantly downslope at short times and axisymmetrically at long times.

One motivation for studying the movement of gravity currents in a porous medium is the process of carbon sequestration, whereby supercritical carbon dioxide ( $\text{CO}_2$ ) is pumped deep underground into porous rock saturated with salt water, which has a greater density. This means that the  $\text{CO}_2$  will rise as a buoyant plume until it reaches an impermeable boundary, at which point it will spread laterally as a gravity current. The Boussinesq approximation means that this is equivalent to a denser fluid moving above an impermeable boundary in a medium saturated with a less dense fluid.

The axisymmetric theory developed by Lyle *et al.* (2005) has been applied to the  $\text{CO}_2$  sequestration site at Sleipner in the North Sea, where several layers of impermeable mudstone have caused injected  $\text{CO}_2$  to accumulate and spread as a series of gravity currents beneath the upper boundaries (Bickle *et al.* 2007). Good agreement was found between observations and model predictions for the propagation rate of individual layers and the thickness of the deeper layers. Our knowledge of geological structure deep underground is limited to data from seismic exploration studies and bore hole data and consequently poorly resolved. In this paper, we develop a theory to help understand to what extent the presence of more complex boundaries, namely channel boundaries, would affect predictions for gravity currents in porous media.

We analyse the flow of gravity currents that have volume given by  $V(t) = Qt^\alpha$ , for some  $Q > 0$  and  $\alpha \geq 0$ , in smooth channels that have uniform cross-section and boundaries defined by  $b(y) \sim a|y/a|^n$ , for some  $n > 0$ , where  $y$  is the cross-channel coordinate and  $a$  is a length scale of the channel. In §2, we lay out the governing equations and state our assumptions. The cases of horizontal and inclined channels are studied separately in §§3 and 4, respectively. For horizontal channels, we use scaling arguments to help derive similarity solutions for the front position and height of the current for general  $\alpha$  and  $n$ . The specific solutions for V-shaped and semicircular channels, both of which were tested against data from

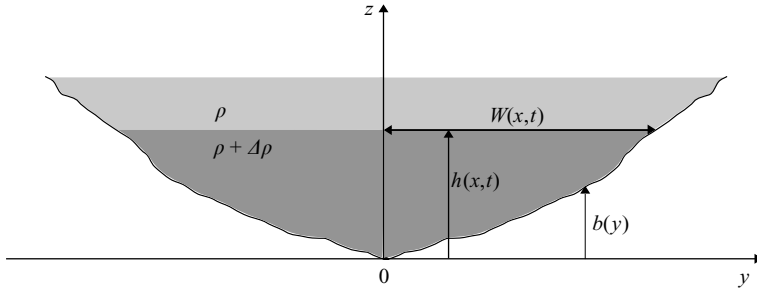


FIGURE 1. Sketch showing the cross-section of an arbitrary channel in the  $y$ - $z$  plane.

specially conducted laboratory experiments, are presented in §§ 3.2.1 and 3.2.2. The experimental results for the two channel shapes, for currents with both constant flux and constant volume, are compared to theoretical predictions in § 3.4. In the case of inclined channels, if the effect of the component of gravity down-channel is much greater than that of the component perpendicular to the channel, scaling analysis in § 4.1 shows that the fluid moves at a constant speed,  $V_f$  say. This is similar to results for two-dimensional (Huppert & Woods 1995) and some initially axisymmetric (Vella & Huppert 2006) gravity currents down an inclined plane. In § 4.2, more general inclined channels are considered and the form of the equation for an equivalent current in a horizontal channel is recovered after changing to a frame of reference moving with speed  $V_f$ . The theoretical model for inclined channels was tested by comparing predictions for front position and height of constant flux gravity currents in an inclined V-shaped channel to experimental and numerical results.

This work is related to publications on the behaviour of low-Reynolds-number gravity currents in open channels without porous media (Takagi & Huppert 2007, 2008, 2010). For channel shapes where  $n \geq 1$ , the effect of the boundary in the porous and non-porous cases is found to be qualitatively similar. However, when  $n < 1$ , the necessity to neglect vertical variations compared with cross-channel variations in the governing equations of the non-porous case and not in the porous case gives rise to a quite different dependency between channel shape and propagation rate. This is discussed in § 3.3. Finally, in § 5 we draw conclusions from the study and suggest a possible application to the problem of CO<sub>2</sub> sequestration.

## 2. Governing equations

Imagine a Newtonian fluid of density  $\rho + \Delta\rho$  ( $\Delta\rho > 0$ ). Propagating in a porous medium saturated with a fluid of lower density  $\rho$ . The gravity current is confined by a lower impermeable channel boundary inclined at an angle  $\theta$  to the horizontal. The channel cross-section is defined by  $z = b(y)$ , independent of  $x$ , where  $x$ ,  $y$  and  $z$  refer, respectively, to the directions down-channel, cross-channel and perpendicular to the slope. The channel geometry is sketched in figure 1. The saturated layer above the current is considered to be sufficiently deep to neglect any motion within it, thus easing calculations, without omitting any essential phenomena. The current is considered to have propagated for long enough time that any pressure differences in the  $y$  direction have levelled its height across the channel and so we treat the fluid height  $h(x, t)$  and width at the top  $2W(x, t)$  as dependent on  $x$  and  $t$  only.

Darcy's law governs the flow of a gravity current in a porous medium (Bear 1988; Phillips 2009)

$$\mathbf{u} = -\frac{k}{\mu}[\nabla p - (\rho + \Delta\rho)\mathbf{g}], \quad (2.1)$$

where  $\mathbf{u}$  is the Darcy velocity,  $p$  is the pressure within the current,  $\mathbf{g} = g(\sin\theta, 0, -\cos\theta)$  the gravitational acceleration,  $k$  is the permeability of the porous medium that is assumed constant and isotropic and  $\mu$  is the dynamic viscosity of the current fluid.

With the assumption that the current is very much longer than it is thick, hydrostatic pressure in the lower layer,  $p(x, z, t)$ , is given by

$$p(x, z, t) = p_0 + p_1(x, t) - (\rho + \Delta\rho)gz \cos\theta, \quad (2.2)$$

where  $p_0$  is a constant reference value and  $p_1(x, t)$  is the hydrostatic pressure in the saturating fluid

$$p_1(x, t) = \rho gx \sin\theta + \Delta\rho gh(x, t) \cos\theta. \quad (2.3)$$

It follows from (2.1) and (2.2) that the  $y$  and  $z$  components of  $\mathbf{u}$  are zero, so there is flow only in the down-channel direction  $x$ , i.e.

$$\mathbf{u} = (u, 0, 0) \quad (2.4)$$

with

$$u = -\frac{kg'}{v} \left( \frac{\partial h}{\partial x} \cos\theta - \sin\theta \right), \quad (2.5)$$

where  $g' = g\Delta\rho/\rho$  is the reduced gravity and  $v = \mu/\rho$ .

Since we assume that  $h$  is independent of  $y$  and  $z$ , it follows from (2.5) that  $u$  is also independent of  $y$  and  $z$ . Thus, the flux  $F$  through cross-sectional area  $A$  may be written as

$$F = 2 \int_0^{W(x,t)} \int_{b(y)}^{h(x,t)} u(x, t) dz dy = uA. \quad (2.6)$$

To be specific, channel boundaries are defined by

$$b(y) = h_c a (y/a)^n, \quad (2.7)$$

where  $n > 0$  is a parameter that specifies the shape,  $a$  is a length scale of the channel width and  $h_c$  is some dimensionless constant of proportionality between channel height and width, defined by (2.8). The fluid height  $h(x, t)$  and width  $W(x, t)$  of gravity currents within such channels are related by

$$h/a = h_c (W/a)^n. \quad (2.8)$$

Condition (2.8) implies that the cross-sectional area of fluid in the current  $A(x, t)$ , at down-channel position  $x$  and time  $t$ , is given by

$$A(x, t) = A_c h^{(1+n)/n}, \quad (2.9)$$

where the constant of proportionality

$$A_c = [2n/(n+1)] h_c^{-1/n} a^{(n-1)/n}. \quad (2.10)$$

Local mass conservation within a medium of uniform porosity  $\phi$  (Huppert & Woods 1995) requires that

$$\phi \frac{\partial A}{\partial t} + \frac{\partial F}{\partial x} = 0. \quad (2.11)$$

Along with (2.6) and (2.9), this yields a governing equation for the current height,

$$\frac{\partial}{\partial t} h^m - S \frac{\partial}{\partial x} \left[ h^m \left( \frac{\partial h}{\partial x} \cos \theta - \sin \theta \right) \right] = 0, \quad (2.12)$$

where  $S = g'k/\phi v$  and  $m = (1 + n)/n$ , and which is independent of the cross-sectional area constant  $A_c$ . Note that as  $n \rightarrow \infty$ ,  $m \rightarrow 1$  and the two-dimensional problem studied by Huppert & Woods (1995) is recovered.

In keeping with previous studies of gravity currents (Huppert 1982), we assume that the total volume in the current at time  $t$  is given by

$$V(t) = Qt^\alpha, \quad (2.13)$$

where  $Q$  is some positive constant and  $\alpha \geq 0$  is a flux parameter, with  $\alpha = 0$  corresponding to constant volume and  $\alpha = 1$  corresponding to constant flux.

Global mass conservation, therefore, requires that

$$\phi \int_0^{x_N(t)} A_c h^m dx = Qt^\alpha \quad (2.14)$$

where  $x_N(t)$  denotes the position of the nose of the current at time  $t$ .

In cases where the term containing the second-order derivative in (2.12) is non-negligible, another boundary condition is imposed on the second-order differential equation by insisting that

$$h[x_N(t), t] = 0. \quad (2.15)$$

This completes the set of governing equations to solve for current height  $h(x, t)$  and front position  $x_N(t)$ .

### 3. Horizontal channels

For horizontal channels,  $\theta = 0$ , the mass conservation equation (2.12) simplifies to

$$\frac{\partial}{\partial t} h^m - S \frac{\partial}{\partial x} \left( h^m \frac{\partial h}{\partial x} \right) = 0. \quad (3.1)$$

#### 3.1. Scaling analysis

In order to help seek similarity solutions, we first use scaling arguments to find how the length scales of the current extent  $L$  and height  $H$  depend on time. We find that they satisfy the relationships

$$L(t) = \kappa t^c \quad \text{and} \quad H(x, t) = \lambda t^d, \quad (3.2a, b)$$

where  $\kappa$ ,  $\lambda$ ,  $c$  and  $d$  are constant scalars for a given current and channel and are determined from the scaling analysis. A similar analysis was carried out by Takagi & Huppert (2008, 2010) for gravity currents in open channels without porous media.

Equations (2.14) and (3.1) provide scaling relationships

$$H^m L/t^\alpha \sim Q/\phi A_c \quad \text{and} \quad L/t \sim SH/L. \quad (3.3a, b)$$

Eliminating  $H$  from (3.3), the scaling for the current length in the down-channel  $x$  direction is found to be

$$L \sim [(Q/\phi A_c)^n S^{n+1}]^{1/(3n+2)} t^c, \quad (3.4)$$

which is a relationship of the form (3.2a) with the power of  $t$  given by

$$c = (\alpha n + n + 1)/(3n + 2). \quad (3.5)$$

This result for  $L$ , inserted into (3.3b), determines the current height scale  $H$  to be

$$H \sim [(Q/\phi A_c)^{2n} S^{-n}]^{1/(3n+2)} t^d, \quad (3.6)$$

which is of the form (3.2b) with

$$d = 2c - 1 = n(2\alpha - 1)/(3n + 2). \quad (3.7)$$

The constant  $Q/\phi A_c$  appears in the scalings for both current length and height and comes from the global mass conservation condition. It represents the ratio between the flux of fluid into the current and the volume of fluid per unit length that can be contained in a cross-section of the channel.

Note that the multiplicative factors  $\kappa$  and  $\lambda$  in (3.2) depend on the physical properties of the porous medium and fluids and on the channel shape parameter  $n$ , but not on the flux parameter  $\alpha$ . The powers of time  $t$ ,  $c$  and  $d$  depend only on the input flux and channel shape parameters  $\alpha$  and  $n$  and not on any other factors. Discussion about these relationships is to be found in §3.3, presented alongside numerical results obtained from the complete similarity solutions derived in the next section.

### 3.2. Similarity solutions

It is possible to find similarity solutions for the height and extent of gravity currents of general input flux  $\alpha \geq 0$  in horizontal channels of general shape  $n > 0$ , which satisfy (3.1) with conditions (2.14) and (2.15). The constraint on  $\alpha$  means that the volume of fluid in the gravity currents under consideration either remains constant or increases with time, while the constraint on  $n$  is required to ensure that the geometrical description is that of a channel.

We obtain from (3.4) a suitable similarity variable  $\eta$ , which for convenience is chosen to be proportional to  $x$

$$\eta = M^{-1/(3n+2)} t^{-c} x, \quad (3.8)$$

where  $M = (Q/\phi A_c)^n S^{n+1}$  and  $c$  is as defined in (3.5).

We seek similarity solutions of the form

$$x_N(t) = \eta_N M^{1/(3n+2)} t^c \quad \text{and} \quad h(x, t) = \eta_N^2 M^{2/(3n+2)} S^{-1} t^d \Psi(y), \quad (3.9a, b)$$

where the prefactors have been chosen using (3.4) and (3.6) to ensure cancellation of dimensional constants in later equations. The powers  $c$  and  $d$  are defined in (3.5) and (3.7) and  $\eta_N$  is a dimensionless scalar equal to the value of  $\eta$  at the current nose  $x = x_N(t)$ . A normalized similarity variable  $y = \eta/\eta_N$  is used in the dimensionless height function  $\Psi$ , again for convenience.

Substituting these expressions into (2.14) and (3.1), with boundary condition (2.15), we obtain the following set of governing equations for the non-dimensional problem.

$$[\Psi^m \Psi'] + [F_1 \Psi + F_2 y \Psi'] \Psi^{m-1} = 0 \quad (3.10a)$$

$$\Psi(1) = 0, \quad (3.10b)$$

$$\eta_N = \left[ \int_0^1 \Psi^m dy \right]^{-1/(2m+1)}, \quad (3.10c)$$

where  $F_1 = (n + 1)(1 - 2\alpha)/(3n + 2)$  and  $F_2 = (n + 1)(\alpha n + n + 1)/n(3n + 2)$ .

These equations can be solved analytically for general  $n$  in the case  $\alpha = 0$ , corresponding to a current of constant volume. Integration of (3.10a) gives the dimensionless height of the current in the channel to be of the parabolic form

$$\Psi(y) = [(n + 1)/(6n + 4)](1 - y^2). \quad (3.11)$$

For other values of  $\alpha$ , numerical methods must be employed to solve (3.10).

In order to apply this general theory to situations we can test experimentally, explicit solutions are derived in the following subsections for V-shaped channels, which correspond to  $n = 1$ , and semicircular channels which may be approximated using  $n = 2$  if the current height is much less than the radius of curvature of the channel. In both cases, when  $\alpha = 0$ , the integral in (3.10c) can be calculated analytically to find  $\eta_N$ .

### 3.2.1. V-shaped channels

A V-shaped channel, with its plane of symmetry along  $y = 0$ , has boundaries defined by  $b(y) = |y|/\tan \beta$ , where  $\beta$  is the angle each channel wall makes with the vertical and corresponds to  $n = 1$  and  $m = 2$  in §2. A gravity current of height  $h$  within the channel has width  $2W(x, t) = 2h \tan \beta$  across the top and cross-sectional area  $A(x, t) = h^2 \tan \beta$ .

The relationships (3.5) and (3.7) indicate the time dependence of the current front position and height to be

$$x_N(t) \sim t^{(\alpha+2)/5} \quad \text{and} \quad h(x, t) \sim t^{(2\alpha-1)/5}. \quad (3.12a, b)$$

When  $\alpha = 0$ ,  $\Psi(y) = (1 - y^2)/5$  from (3.11) and analytical integration of (3.10c) gives  $\eta_N = (375/8)^{1/5} = 2.159 \dots$ . Hence, the similarity solutions (3.9) for the front position of the current and height of a finite release of fluid into a V-shaped channel may be written explicitly as

$$x_N(t) = \left( \frac{375g^2k^2Q}{8\phi^3v^2 \tan \beta} \right)^{1/5} t^{2/5} \quad (3.13)$$

and

$$h(x, t) = (\phi v / 5g'k) (x_N^2 - x^2) t^{-1} \quad (0 < x < x_N). \quad (3.14)$$

For  $\alpha > 0$ , the unknown quantities  $\eta_N$  and  $\Psi(y)$  in the full solution need to be calculated numerically.

### 3.2.2. Semicircular channels

Similarly, a channel with a semicircular cross-section, radius  $R$ , with its plane of symmetry aligned with  $y = 0$  can be considered. If we assume that  $R$  is very large compared with the scale of the fluid height  $h = h(x, t)$ , such that  $h/R \ll 1$  and  $W/R \ll 1$ , then the channel boundaries may be approximated by the first term of the Taylor expansion for an exactly semicircular boundary,  $b(y) \approx y^2/2R$ . This geometry corresponds to  $n = 2$ ,  $m = 3/2$  and length scale  $a = 2R$  in §2. The width of the current across the top  $2W(x, t) = 2(2Rh)^{1/2}$  and its cross-sectional area  $A = 4(2Rh^3)^{1/2}/3 \equiv A_c h^{3/2}$ .

In such channels, (3.5) and (3.7) indicate that

$$x_N(t) \sim t^{(2\alpha+3)/8} \quad \text{and} \quad h(x, t) \sim t^{(2\alpha-1)/4}. \quad (3.15a, b)$$

When  $\alpha = 0$ , (3.11) gives  $\Psi(y) = 3(1 - y^2)/16$  and  $\eta_N = 4(16/243\pi^2)^{1/8} = 2.138 \dots$  from (3.10c). Hence, the explicit similarity solutions for the nose position of the

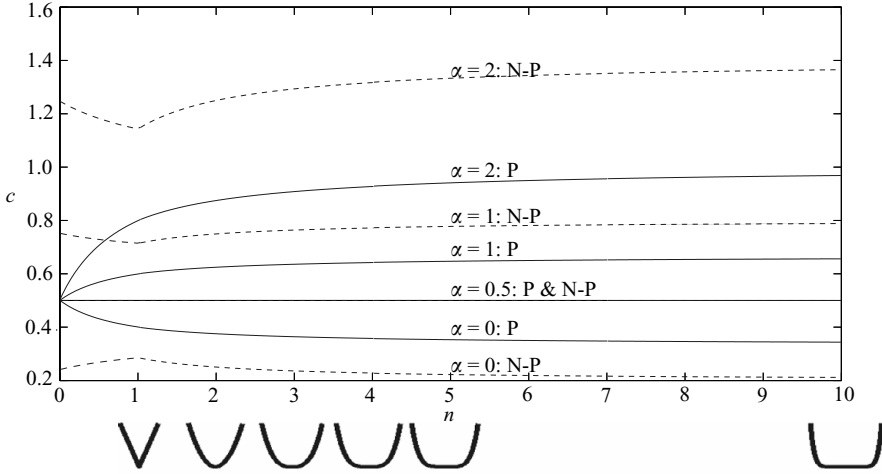


FIGURE 2. The value of  $c$ , for a current with length  $L \sim t^c$  and volume  $V \sim t^\alpha$  in a channel that has a boundary  $b \sim a|y/a|^n$ , as a function of  $n$  for different values of  $\alpha$  in horizontal channels. Results for channels in porous media are represented by solid lines and annotation P and results for open channels without porous media are represented by dashed lines and N-P. The channel shapes corresponding to various values of  $n$  are sketched in the appropriate places below the  $n$ -axis.

current and height of a finite release of fluid in a horizontal semicircular channel, from (3.9), are

$$x_N(t) = 4 \left( \frac{g^3 k^3 Q^2}{54\pi^2 R \phi^5 \nu^3} \right)^{1/8} t^{3/8} \quad (3.16)$$

and

$$h(x, t) = (3\phi\nu/16g'k) (x_N^2 - x^2) t^{-1} \quad (0 < x < x_N). \quad (3.17)$$

### 3.3. Numerical results and discussion

The time exponent of the speed of propagation of a gravity current in a channel is determined by the value of  $c$  described in (3.5) and is a function of the parameter governing the time rate of change of the fluid volume  $\alpha$  and the shape of the boundary wall governed by  $n$ . Figure 2 displays how  $c$  depends on  $n$  for various values of  $\alpha$ . The effect of increasing the channel shape parameter  $n$ , i.e. the effect of opening up the channel boundary to the horizontal, is determined by whether  $\alpha$  is greater or less than a critical value  $\alpha_c$ , which is directly due to global conservation of mass. Equation (3.5) implies that the current length will always increase with time. If the current height at a particular point is increasing, more fluid will be required to maintain the increase when  $n$  is higher and so the length of the flow will increase at a slower rate with increased  $n$ . By the same argument, the converse is true for a height which is decreasing. Equation (3.7) indicates that above the critical value  $\alpha_c = 1/2$  the current height increases and below  $\alpha_c$  the current height diminishes with time.

For many applications, for example the study of the long-term extent of a volume of  $\text{CO}_2$  moving as a gravity current within a channel in a reservoir cap rock, it is of particular interest to know whether the current front is accelerating, decelerating or propagating at a constant speed, i.e. whether  $c > 1$ ,  $c < 1$  or  $c = 1$ . As the time rate of change of the current volume  $\alpha$  increases, the propagation rate increases linearly for a fixed channel shape  $n$ . This increased propagation rate would be expected when



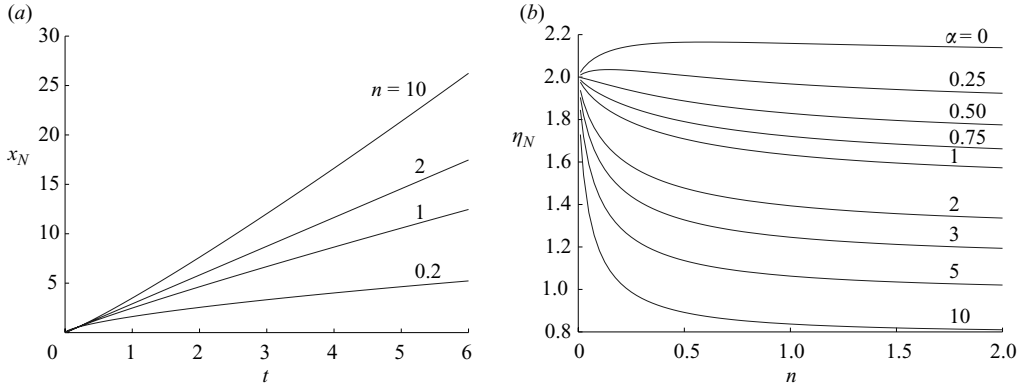


FIGURE 3. Numerical results for gravity currents in channels. (a) The behaviour of current propagation when  $\alpha = 2.5$  in different shaped channels. (b) The value of  $\eta_N$  as a function of  $n$  for various values of  $\alpha$ .

there is more fluid being supplied to drive the current forward. For  $\alpha < 1/2$ , although  $c$  increases as  $n$  decreases, it is always true that  $c < 1/2$ . When  $\alpha = 1/2$ ,  $c = 1/2$  regardless of channel shape. However, if the current volume increases rapidly enough, specifically if  $\alpha > 1/2$ , and the channel shape is such that  $n \geq 1$ , the effect of boundary shape on the current propagation rate  $c$ , for any fixed  $\alpha$ , varies quite significantly in three distinct ranges of  $\alpha$ . The regimes are (i)  $0.5 < \alpha \leq 2$ , (ii)  $2 < \alpha \leq 3$  and (iii)  $3 < \alpha$ . Gravity currents in channels with  $0 < n < 1$  exhibit slightly different dependence on  $\alpha$  and so will be considered separately.

Darcy's law implies that the Darcy velocity  $U \sim L/t$  of the current is directly proportional to the pressure gradient, which under the hydrostatic assumption scales like the aspect ratio of the current  $A_R = H/L$ . The length scales  $L$  and  $H$  are, as before, in the directions down-channel and perpendicular to the channel. For this reason, in order to understand the dependence of  $c$ , where  $L \sim t^c$ , on  $\alpha$  and  $n$ , it is useful to consider how  $A_R$  and therefore the pressure gradient driving the motion, changes with time. Equations (3.5) and (3.7) imply that

$$A_R \sim t^{(n(\alpha-2)-1)/(3n+2)}. \quad (3.18)$$

Therefore, in regime (i),  $1/2 < \alpha \leq 2$ , even though the current height is increasing with respect to time and so an increase in  $n$  causes an increase in  $c$ , the aspect ratio is decreasing with respect to time. Hence, from (3.3b), the pressure gradient will never increase enough to make  $L$  propagate at a faster rate than  $t$ . In regime (ii), when  $2 < \alpha \leq 3$ ,  $H/L$  can increase with respect to time if  $n$  is large enough, i.e. if the channel base is flattened enough, to make the power of  $t$  positive in (3.18). This means that the pressure gradient is increasing with respect to time and so the current is able to accelerate. This is illustrated in figure 3 for  $\alpha = 2.5$  when the current length increases as  $t^{9/10}$  in a V-shaped channel ( $n = 1$ ), as  $t$  in an approximately semicircular shaped channel ( $n = 2$ ) and accelerates with respect to  $t$  for higher values of  $n$ . In regime (iii), where  $3 < \alpha$  and  $n \geq 1$ , the input flux is increasing sufficiently rapidly to ensure that the position of the current front is always accelerating.

When  $0 < n < 1$ , the rate of propagation shows high sensitivity to changes in  $n$ . This reflects the greater sensitivity of boundary shape to small changes in  $n$  compared to when  $n \geq 1$ . Regardless of the channel shape, (3.18) indicates that if  $\alpha \leq 3$ , the pressure gradient of the current will never be sufficient to cause the current front to accelerate.

However, for any narrow channel described by  $n$  in the range  $(0, 1)$ , if the time rate of change of the input flux  $\alpha > 3$  is high enough, the current will propagate at a faster rate than  $t$ . Such a scenario could be possible in the initial stages of injection of  $\text{CO}_2$  into a reservoir, but unlikely at later times because the injection rate slows down as storage capacity is used up.

In the limiting case  $n \rightarrow \infty$ , the channel has a rectangular cross-section, so ignoring the effects from sidewalls, the flow will be two-dimensional. Towards this limit,  $c \rightarrow (\alpha + 1)/3$ , in agreement with the result found by Huppert & Woods (1995) for a two-dimensional gravity current in a porous medium propagating over a flat horizontal boundary.

The values of  $c$  as a function of  $n$  for various values of  $\alpha$  for gravity currents in open channels without porous media (Takagi & Huppert 2008) are displayed in figure 2 alongside the equivalent values of  $c$  found in this work on channels in porous media. The critical value of  $\alpha$  which divides the two regions in which  $c$  varies in opposing ways with  $n$  is the same in both cases since it is determined by the equation of global mass conservation, which up to a factor of porosity  $\phi$  is common to both. For  $n \geq 1$ , the behaviour of  $c$  is qualitatively similar in both cases. The value of  $c$  is linear in  $\alpha$  in both porous and non-porous cases with the different gradients determined by the Darcy and Navier–Stokes momentum equations, respectively. The difference between behaviours for  $n < 1$  is due to the fact in the porous case there is no  $\nabla^2$  term and so no assumption needs to be made about the relative magnitude of the cross-channel and vertical length scales.

The value of the similarity variable at the current nose  $\eta_N$ , which appears in the similarity solutions (3.9), is plotted in figure 3(b) as a function of  $n$  for various values of  $\alpha$ . For all channel shapes,  $\eta_N$  increases with decreasing  $\alpha$ . As  $n$  approaches zero,  $\eta_N$  approaches the critical value  $\eta_N^c = \eta_N(\alpha = 0.5)$  regardless of  $\alpha$ , which is a consequence of the powers of time in the similarity solutions (3.9) approaching critical values,  $c^c = 0.5$  and  $d^c = 0$ , for all  $\alpha$  as  $n \rightarrow 0$ . For  $\alpha > 0.5$ ,  $\eta_N$  increases as  $n$  decreases and similarly for  $\alpha < 0.5$ ,  $\eta_N$  increases very slightly as  $n$  decreases except for very small values as  $n \rightarrow 0$  where  $\eta_N$  decreases to the limiting value  $\eta_N^c$ . For  $n \geq 1$ , the influence on  $\eta_N$  of changing the channel shape parameter  $n$  is much less than changing the input flux parameter  $\alpha$ , with the effect on  $\eta_N$  of changing either parameter becoming smaller as they increase. Physically, this indicates that  $\eta_N$  is more sensitive to changes in input flux and channel shape when the rate of increase of the volume of fluid in the current is smaller and it flows within narrower channels.

### 3.4. *Experimental results*

To validate the theory developed for horizontal channels, we conducted a series of laboratory experiments in V-shaped and semicircular channels and compared the results with the specific similarity solutions derived in §§3.2.1 and 3.2.2. For both channel shapes, we tested the cases of currents with constant volume ( $\alpha = 0$ ) and constant flux ( $\alpha = 1$ ).

In the case of a V-shaped channel, a Perspex tube of triangular cross-section with angle  $\beta = \pi/4$  between each sloping boundary and the vertical was fixed between two Perspex end plates. Similarly, to create a semicircular channel, a cylindrical Perspex tube of radius 5.75 cm and length 88 cm was glued between two Perspex end plates. A nozzle at the bottom of one end plate allowed fluid to be injected into the tank, while a hole at the top of the plate at the opposite end allowed displaced fluid to exit freely. To create a porous medium, each tank was filled with 2 mm diameter glass

| Constant volume |                        |                  |        | Constant flux |                        |                                 |        |
|-----------------|------------------------|------------------|--------|---------------|------------------------|---------------------------------|--------|
| Experiment      | $g'(\text{cm s}^{-2})$ | $Q(\text{cm}^3)$ | Symbol | Experiment    | $g'(\text{cm s}^{-2})$ | $Q(\text{cm}^3 \text{ s}^{-1})$ | Symbol |
| S1              | 73                     | 103              | □      | Sa            | 57                     | 1.28                            | *      |
| S2              | 75                     | 80               | ○      | Sb            | 57                     | 0.57                            | ○      |
| S3              | 41                     | 85               | △      | Sc            | 57                     | 0.46                            | □      |
|                 |                        |                  |        | Sd            | 75                     | 0.24                            | △      |
| V1              | 20                     | 200              | +      | Va            | 44                     | 0.20                            | ●      |
| V2              | 60                     | 100              | ×      | Vb            | 75                     | 0.25                            |        |
| V3              | 40                     | 150              | ●      |               |                        |                                 |        |
| V4              | 40                     | 62               |        |               |                        |                                 |        |

TABLE 1. Parameter values and symbols used for the experiments represented in figure 4. *S* and *V* denote experiments in semicircular and V-shaped channels, respectively.

| Channel shape | Constant volume   |                      | Constant flux     |                                   |
|---------------|-------------------|----------------------|-------------------|-----------------------------------|
|               | $t \sim$          | $x \sim$             | $t \sim$          | $x \sim$                          |
| V-shaped      | $\nu/(g'Q^{1/3})$ | $(k^2Q^{1/3})^{1/5}$ | $\nu/(g'k^{1/2})$ | $(\nu Qk^{1/2}/g')^{1/5}$         |
| Semicircular  | $\nu/(g'R)$       | $(k^3Q^2/R^4)^{1/8}$ | $\nu/(g'k^{1/2})$ | $(Q^2\nu^2k^{1/2}/(Rg'^2))^{1/8}$ |

TABLE 2. Combinations of parameters used to non-dimensionalize experimental results.

ballotini. Before each experiment, the ballotini in the tank were saturated with water at room temperature.

A dense salt solution coloured blue with food dye was delivered from a beaker 1 m above the tank to the input nozzle via a siphon. The beaker sat on a digital mass balance linked to a computer and thus the mass of fluid entering the tank was accurately recorded as a function of time. The gravity feed was controlled by an on-off tap and the rate of fluid flow could be adjusted using a control valve.

The parameters representing porosity  $\phi$ , permeability  $k$  and kinematic viscosity  $\nu$  were held constant across all our experiments. Further discussion of the values of  $\phi$  and  $k$  for closely packed spherical glass beads of diameter 2 mm is given by Acton, Huppert & Worster (2001). The values used by Acton *et al.* (2001) to non-dimensionalize experimental results are  $\phi = 0.37$  and  $k = 3.1 \times 10^{-5} \text{ cm}^2$  and these values are used for analysing experiments in this paper.

In order to test the scalings in the multiplicative factors in similarity solutions (3.9), we varied the reduced gravity  $g'$  and volume parameter  $Q$  between experiments. The values used in each experiment are summarized in table 1. The combinations of parameters used for non-dimensionalization of experimental results are summarized in table 2.

### 3.4.1. Constant flux

Constant flux gravity currents were created by allowing the gravity-fed flow of dyed salt solution to enter the tank, with the flux  $Q$  set using the control valve. The non-dimensional results for current front position against time in both V-shaped and semicircular channels are plotted in figure 4(a). After a small amount of time, the results for both channels tend towards the theoretical similarity solution represented by the solid line. This indicates good agreement for the powers of time

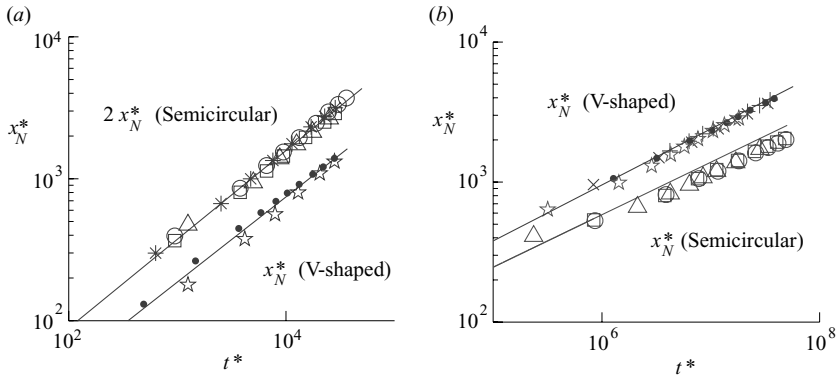


FIGURE 4. Experimental results for gravity currents of (a) constant flux and (b) constant volume in the horizontal V-shaped and semicircular channels. The non-dimensional front position  $x_N^*$  is plotted against non-dimensional time  $t^*$ . The parameter values and corresponding symbols for these experiments are summarized in table 1. Note that the measurements of front position in the semicircular channel in figure 4(a) have been multiplied by a factor of 2 in order that they be separated from the data for the V-shaped channel.

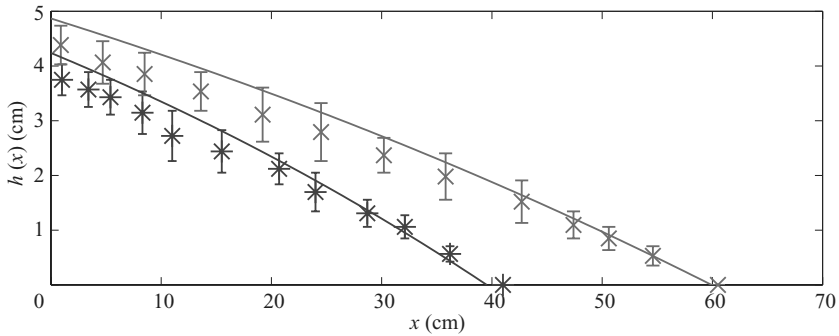


FIGURE 5. Experimental results with error bars for the current height measured after 8 (\*) and 16 (x) minutes in experiment *Va*, a constant flux gravity current in a horizontal V-shaped channel. Solid curves represent theoretical predictions.

$t^{3/5}$  and  $t^{5/8}$  for V-shaped and semicircular channels, respectively. The collapse onto the theoretical lines also indicates very good agreement with the pre-multiplicative factors in the similarity solutions, where any difference may be acceptably explained by experimental measurement error.

Dispersion occurs as a fluid moves through the interstices of a porous medium (see e.g. Phillips 2009). This causes a fuzzy region at the interface between the dyed salt solution and surrounding water, which will inevitably result in some difference between experimental measurements and theoretical predictions. For experiment *Va*, involving a constant flux gravity current in a V-shaped channel, measurements of current height were taken at the top and bottom of the fuzzy region after 8 and 16 minutes. The averages of these measured heights at each time are plotted in figure 5 as a function of down-channel position  $x$ , with error bars reflecting the thickness of the region of dispersion. The theoretical predictions are plotted as solid curves and at both times the curves lie nearly always within the error bars of the experimental results, indicating satisfactory agreement with the similarity solution. The theoretical predictions lie close to the measured upper bounds of the current height for most of

its length, except towards the nose. This suggests that the hydrodynamic dispersion that is taking place at the boundary of these constant flux gravity currents causes most mixing to occur at the front of the current, which is similar to the position of entrainment at the head of a turbulent gravity current (Hallworth *et al.* 1996).

### 3.4.2. Constant volume

For all constant volume gravity currents in the semicircular channel and experiment V4 in the V-shaped channel, a finite volume of salt solution was fed to the tank via a constant flux lasting approximately 30 seconds. The volume of fluid  $Q$  was derived using the mass measurements of the reservoir before and after input and the known density of the solution. The time origin used for the resulting current was the time at which the gravity feed was turned off and after which the current volume was constant. Experiments V1, V2 and V3 were conducted in a different tank corresponding again to a V-shaped channel with  $\beta = \pi/4$ , but this time with a section of ballotini saturated with salt solution separated from the main region of ballotini saturated with water, by a gate that was pulled up at time  $t = 0$ .

The non-dimensional results for current nose position as a function of time for all the constant volume experiments are plotted in figure 4(b). The solid lines represent the similarity solution in each case. The experimental data for the V-shaped channel show good agreement to the theoretical time dependence  $t^{2/5}$  and pre-multiplicative factor in (3.13). The fact that the results from both V-shaped tanks all tend to the similarity solution strengthens the validity of the theory and highlights its independence from initial conditions.

While the results for the semicircular tank show satisfactory agreement to the theoretical time dependence  $t^{3/8}$  in (3.16), they do not show quite as good agreement with the pre-multiplicative factor. The propagation of the current is 20 % slower than predicted in these experiments, which is consistent with a current of smaller volume  $Q$  or lower reduced gravity  $g'$ . Smaller volume could reflect the fact that a non-trivial proportion of the salt solution remains temporarily trapped against the channel sides as the current height decreases from its initial highest value. This effect is exaggerated in the semicircular channel because the walls are less steep than those in the V-shaped channel. With constant flux gravity currents, the current height increases at any fixed position and so this phenomenon would not occur.

## 4. Inclined channels

For inclined channels, the full local mass conservation equation (2.12) must be solved along with the global mass constraint (2.14) and boundary condition (2.15).

### 4.1. Channels inclined by a large angle ( $\tan \theta \gg \partial h / \partial x$ )

When the channel slope is much greater than the slope of the free surface, i.e.  $\tan \theta \gg \partial h / \partial x$ , the current is driven by the downslope component of gravity and not by the pressure gradient due to variations in the height of the current. It is possible in such cases to neglect the term with the second-order derivative in (2.12), thus obtaining the governing equation

$$\frac{\partial}{\partial t} h^m + S \sin \theta \frac{\partial}{\partial x} h^m = 0. \quad (4.1)$$

As in §3.1, scaling relations can be used to help construct solutions. Hence, using the same notation for the scales as before, we obtain from (2.14) and (4.1)

$$H^m L/t^\alpha \sim Q/\phi A_c \quad \text{and} \quad 1/t \sim S \sin \theta/L. \quad (4.2a, b)$$

Equation (4.2b) alone indicates that regardless of flux parameter  $\alpha$  or channel shape parameter  $n$ , the length of the current  $L \sim St \sin \theta$ . This agrees with the result for a two-dimensional gravity current, corresponding to the limit  $m \rightarrow 1$ , down an inclined plane (Huppert & Woods 1995) and shows that a gravity current flowing down a channel that has a slope much steeper than its free surface is not affected by confining boundaries.

Furthermore, in a frame moving with speed  $S \sin \theta$ , the current height remains constant.

#### 4.2. General inclined channels

In general, where the effect of the pressure gradient due to the slope of the free surface may not be neglected as happens in §4.1, it helps greatly to change to a frame moving with speed  $S \sin \theta$  in order to solve the complete governing equations (Huppert & Woods 1995). Rewriting (2.12) in terms of the down-channel coordinate in the moving frame  $x' = x - St \sin \theta$ , we obtain

$$\frac{\partial}{\partial t} h^m - S \cos \theta \frac{\partial}{\partial x'} \left( h^m \frac{\partial h}{\partial x'} \right) = 0, \quad (4.3)$$

and (2.14) becomes

$$\phi \int_{-St \sin \theta}^{x'_N(t)} A_c h^m dx' = Qt^\alpha, \quad (4.4)$$

where  $x'_N(t)$  denotes the position of the nose of the current in the moving frame at time  $t$ . Equation (4.3) is the same equation as the mass conservation equation in the horizontal case (3.1), with  $S$  changed to  $S \cos \theta$ , as in Huppert & Woods (1995).

Therefore, the action of gravity in the downslope direction is unaffected by channel shape, while its effect in the direction perpendicular to the slope is similar to that for flow in an equivalent horizontal channel.

##### 4.2.1. Constant flux gravity current, $\alpha = 1$

The case of a constant flux gravity current is interesting because both the fluid input flux and the propagation due to gravity parallel to the down-slope direction scale like  $t$ . For such a current, where fluid is released at position  $x_0$ , the solution for height and nose position in the initial stages must be found by numerical solution of the full equations. To do this, we note that if  $h \sim h_0 f$  for some height scale  $h_0$  and non-dimensional function  $f$ , scaling of (4.3) indicates that, within the moving frame, the current length scale  $L' \sim (Sh_0 t \cos \theta)^{1/2}$  (Huppert & Woods 1995). Equation (4.3) can then be solved using the similarity variable  $\eta = x'/(Sh_0 t \cos \theta)^{1/2}$ , choosing  $h_0$  such that condition (4.4) is met. However, after sufficiently long time, the component of gravity down-slope dominates, since  $St \sin \theta \gg (Sh_0 t \cos \theta)^{1/2}$ , causing the current nose to move almost at the rate at which the fluid is being injected. The current height therefore tends to a fixed depth  $h_f$  except at the nose, where gravity perpendicular to the slope smoothes the height to zero (Huppert & Woods 1995). Global mass conservation implies that this fixed depth for the majority of the current length is given by

$$h_f = \left[ \frac{Q}{\phi A_c} \frac{1}{S \sin \theta} \right]^{n/(n+1)}. \quad (4.5)$$

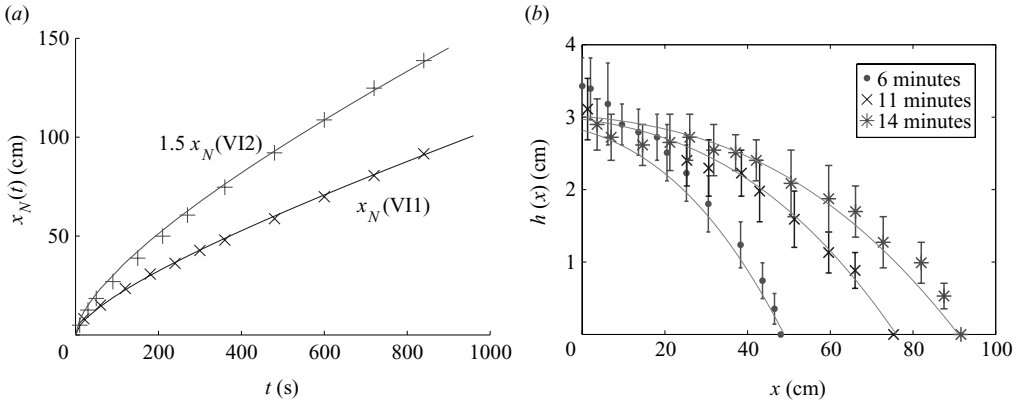


FIGURE 6. Data from experiments for a constant flux gravity current in a V-shaped channel inclined at  $\theta = 9^\circ$ , VII ( $Q = 0.20 \text{ cm}^3 \text{ s}^{-1}$ ,  $g' = 44 \text{ cm s}^{-2}$ ) and VI2 ( $Q = 0.55 \text{ cm}^3 \text{ s}^{-1}$ ,  $g' = 35 \text{ cm s}^{-2}$ ). (a) Current nose position against time for experiments VII( $\times$ ) and VI2( $+$ ). The solid lines represent theoretical results. Note that the results for the front position in experiment VI2 have been multiplied by a factor 1.5 so that they are separated from the data for experiment VII. (b) Current height in experiment VII with error bars against down-channel position at three different times. The solid curves represent the theoretical height at each time.

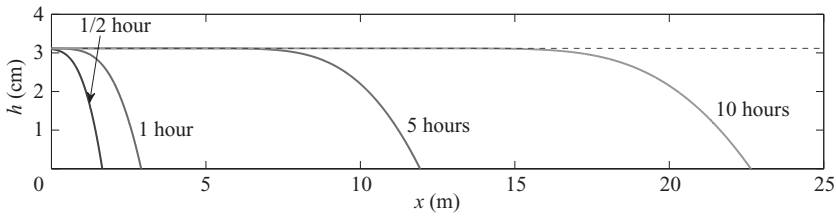


FIGURE 7. Numerical solution for the height profile of the gravity current in experiment VII after long times. The dotted line represents the predicted long time fixed depth of the current.

In order to verify this theory, we conducted two experiments with a constant flux gravity current down an inclined V-shaped channel, varying the flux  $Q$  and reduced gravity  $g'$  between each run. The apparatus was set up as described in §3.4, but with the channel inclined at an angle  $\theta = 9^\circ$ . The experimental values of  $Q$  and  $g'$  are displayed in figure 6. Results for current nose position against time are plotted in figure 6(a), along with the theoretical predictions obtained by numerical solution of (4.3), (4.4) and the condition  $h[x'_N(t)] = 0$ . The two sets of results for each experiment are in very good agreement.

The experimental results recorded for the height of the current after 6, 11 and 14 minutes are plotted in figure 6(b). As for the results for the horizontal channel, because of the dispersion of fluid moving through a porous medium, a fuzzy region at the top of the current was observed in the experiment, reflected by error bars on the graph. Their average position is plotted by the markers. The numerical solutions of the full set of equations for current height at each time are represented by solid curves and lie almost everywhere within the error bars at each time. Figure 7 displays a plot of the numerical solution for the height of the same current after longer times, namely 0.5, 1, 5 and 10 hours. Note that our experimental tank was not long enough to obtain experimental data for these times. The dotted line shows  $h = h_f = 3.12$ , the long-term fixed depth as predicted by (4.5) for the given experimental parameters. It

verifies that the current does indeed tend to this fixed depth for the majority of its length after a long enough time.

## 5. Conclusion

In this study, we have investigated theoretically and experimentally how the propagation and form of gravity currents that have volume  $V \sim t^\alpha$ , flowing along channels that have boundary walls defined by  $b \sim a|y/a|^n$ , are affected by varying  $\alpha$  and  $n$ .

A scaling analysis that was used to construct similarity solutions indicates that, if the current length scales like  $L \sim t^c$ , in a horizontal channel,  $c = (\alpha n + n + 1)/(3n + 2)$ . We find that there is a critical value for the volume parameter  $\alpha$ ,  $\alpha_c = 1/2$ , below which the propagation of a current within a horizontal channel decreases as  $n$  increases because the current height is decreasing with respect to time, and above which the current becomes faster as  $n$  increases because the height is increasing with respect to time. The physical interpretation of this is that gravity currents with volumes that are constant or increasing slowly with respect to time propagate faster in narrower channels, but when the rate of increase of fluid volume becomes higher, the current front propagates faster with respect to time in channels with flatter bottoms.

Experimental data for constant flux gravity currents in V-shaped and semicircular channels and for constant volume currents in V-shaped channels agree well with the theory for both current nose position and height profile. Results for experiments involving constant volume gravity currents in a semicircular channel showed that the current propagation is slightly slower than expected, which might just be explained by loss of volume from the current due to hindered drainage on the channel sides as the current height decreases.

In an inclined channel, the effect of the component of gravity in the downslope direction is to cause the gravity current to propagate at a constant speed  $S \sin \theta$ , regardless of  $\alpha$  and  $n$ , as for a two-dimensional current (Huppert & Woods 1995) and some initially axisymmetric currents (Vella & Huppert 2006) down an inclined plane. When the slope of the channel is much larger than that of the free surface, i.e. when  $\tan \theta \gg \partial h / \partial x$ , this component of gravity dominates. Therefore, in these cases, the channel shape has negligible effect on the motion of the current. For more general channels, the effect of the component of gravity perpendicular to the channel acting on variations in the height of the current free surface is non-negligible and the full governing equations must be solved numerically. By changing to a reference frame moving with speed  $S \sin \theta$ , the form of the governing equation for a corresponding gravity current in a horizontal channel is obtained. A constant flux gravity current in an inclined channel will tend to a constant depth for times  $t \gg h_f \cot \theta / S \sin \theta$ , where  $h_f$  is given by (4.5). The boundary layer at the front of the current, in which the height changes smoothly from the fixed depth  $h_f$  to zero, grows in the moving frame as  $(Sh_f t \cos \theta)^{1/2}$ , which recovers the result for two-dimensional gravity currents when  $m = 1$  (Huppert & Woods 1995). Experimental data for a constant flux gravity current down an inclined V-shaped channel showed very good agreement to theoretical predictions for height and front position.

Finally, we return to the motivation of CO<sub>2</sub> sequestration and suggest a relevant application of this study. Bickle *et al.* (2007) suggested that the topography of the impermeable mudstone layers at the CO<sub>2</sub> sequestration site at Sleipner is a possible reason for the observed elliptical shape of the gravity currents spreading beneath them. Our findings indicate that a mass of carbon dioxide for which  $\alpha \leq 1$ , propagating



beneath a horizontal caprock, will always move faster if it is confined within a channel than it would in an axisymmetric geometry, with currents moving faster in narrower or flatter based channels depending on the rate of increase of their volume. Alternatively, if the rate of increase of the current volume in a layer were increasing such that  $\alpha > 1$ , certain narrow channel shapes could cause the fluid to propagate more slowly than in the axisymmetric case. This shows that the presence of channels in the impermeable clay layers could cause the CO<sub>2</sub> to flow faster in a particular direction and produce a non-axisymmetric shape such as the elliptical gravity currents observed at Sleipner.

We gratefully acknowledge Mark Hallworth for his invaluable assistance in the laboratory. The research of M.J.G. is funded by the EPSRC and the research of H.E.H. is partially supported by a Royal Society Wolfson Research Merit Award.

#### REFERENCES

- ACTON, J. M., HUPPERT, H. E. & WORSTER, M. G. 2001 Two-dimensional viscous gravity currents flowing over a deep porous medium. *J. Fluid Mech.* **440**, 359–380.
- BEAR, J. 1988 *Dynamics of Fluids in Porous Media*. Dover.
- BICKLE, M., CHADWICK, A., HUPPERT, H. E., HALLWORTH, M. & LYLE, S. 2007 Modelling carbon dioxide accumulation at Sleipner: implications for underground carbon storage. *EPSL* **255**, 164–176.
- HALLWORTH, M. A., HUPPERT, H. E., PHILLIPS, J. C. & SPARKS, R. S. J. 1996 Entrainment into two-dimensional and axisymmetric turbulent gravity currents. *J. Fluid Mech.* **308**, 289–311.
- HUPPERT, H. E. 1982 The propagation of two-dimensional and axisymmetric viscous gravity currents over a rigid horizontal surface. *J. Fluid Mech.* **121**, 43–58.
- HUPPERT, H. E. 2006 Gravity currents: a personal perspective. *J. Fluid Mech.* **554**, 299–322.
- HUPPERT, H. E. & WOODS, A. W. 1995 Gravity-driven flows in porous layers. *J. Fluid Mech.* **292**, 55–69.
- LYLE, S., HUPPERT, H. E., HALLWORTH, M., BICKLE, M. & CHADWICK, A. 2005 Axisymmetric gravity currents in a porous medium. *J. Fluid Mech.* **543**, 293–302.
- PHILLIPS, O. M. 2009 *Geological Fluid Dynamics: Sub-Surface Flow and Reactions*. Cambridge University Press.
- SIMPSON, J. E. 1997 *Gravity Currents: In the Environment and the Laboratory*. Cambridge University Press.
- TAKAGI, D. & HUPPERT, H. E. 2007 The effect of confining boundaries on viscous gravity currents. *J. Fluid Mech.* **577**, 495–505.
- TAKAGI, D. & HUPPERT, H. E. 2008 Viscous gravity currents inside confining channels and fractures. *Phys. Fluids* **20**.
- TAKAGI, D. & HUPPERT, H. E. 2010 Initial advance of lava flows in open channels. *J. Volcanol. Geotherm. Res.* (submitted).
- VELLA, D. & HUPPERT, H. E. 2006 Gravity currents in a porous medium at an inclined plane. *J. Fluid Mech.* **555**, 353–362.